01 Jan 1973

Measurements of Pulsating Turbulent Water Flow in a Tube

S.-Z. Lu

R. J. Nunge

F. F. Erian

M. Mohajery

MEASUREMENTS OF PULSATING TURBULENT WATER FLOW IN A TUBE

S.-Z. Lu and R. J. Nunge, Department of Chemical Engineering
F. F. Erian and M. Mohajery, Department of Mechanical Engineering
Clarkson College of Technology, Potsdam, N. Y. 13676

ABSTRACT

The experimental method associated with obtaining meaningful information from the hot-film anemometer signals in fully developed pulsating turbulent flow where the pulsations are sinusoidal in time is discussed. The results of a number of experiments in water reveal the nature of the long-time and short-time average velocity and pressure. Velocity measurements between 0.95 radii and the centerline demonstrate that the long-time average velocity distribution is coincident with that for steady turbulent flow at the same Reynolds number. Also, no significant differences between the long-time average axial pressure drop in the pulsating and steady flows were noted, although this requires further investigation in view of the increases in the Reynolds stress observed in pulsating air flow.

The distribution of the measured pulsating velocity component depends upon the dimensionless turbulent frequency. At the lowest values of the frequency, the profile is turbulent-like, while at higher values, the maximum in the velocity shifts from the centerline towards the wall and a uniform speed region exists over the central portion of the tube.

An eddy viscosity model displays many of the important characteristics of the observed pulsating velocity. Using the results of this model and the experimental observations, limits of the laminar frequency parameter which delineates the response of the flow are suggested.

Recordings of the instantaneous velocity signal suggest the short-time behavior of the axial turbulence intensity to be generally that of increasing during deceleration of the flow and decreasing during acceleration.

INTRODUCTION

The problem of unsteady flow is a very general one, since regular and irregular oscillations occur widely in nature and in industry. The behavior of pulsating laminar flow in a cylindrical pipe away from the region affected by the ends is well understood (6,12,19). However, existing knowledge of pulsating turbulent flow is limited.

One of the earliest investigators in this field was Schultz-Grunow (17) who found from experiments that the time averaged friction factor for pulsating turbulent flow did not differ considerably from the steady flow value. That is, the instantaneous frictional loss could be predicted from the instantaneous mean velocity and steady flow friction factor, thus suggesting a quasi-steady behavior.

Recently, the quasi-steady model was further investigated by several investigators (1, 11, 18). However, at least two important questions have not been discussed in sufficient detail by the above authors: first, what are the parameter ranges in which the quasi-steady model applies; and second, what are the critical parameters for understanding pulsating turbulent flows?

An answer to the first question was attempted by Brown et al. (4), who provided an analytical development for the frequency response to small amplitude fluctuations. Three frequency regimes were suggested: for low frequency pulsations, the flow is quasi-steady; for high frequency pulsations the flow is stationary or frozen; and for intermediate frequency pulsations, the eddy viscosity profile changes in a complex way. The intermediate frequency range was suggested to be $0.01\ Re_s < \frac{\omega R^2}{\nu} < 0.1\ Re_s$ with a break frequency of about $0.025\ Re_s$. However, Brown et al. neglected the acceleration term, $\partial\bar{U}/\partial t$, in the quasi-steady model equation for the first regime. This approximation may lead to an underestimation of the frequency range in which the quasi-steady model applies (13).

The second question was addressed by Karlsson (8) who conducted an experimental investigation of pulsating parallel flow in a wind tunnel system. Karlsson found that when the pulsation amplitude is less than about 35%, there is no effect of the amplitude on the unsteady component of pulsating velocity. That is, if the local unsteady component of pulsating velocity is made dimensionless by the centerline unsteady component of the pulsating velocity, the resulting dimensionless velocity is independent of the pulsation amplitude over the frequency range of 0 to 48 cycles/sec.

The effect of the pulsation frequency on the mean flow structure was studied by Gerrard (7) and Karlsson (8). Each of these workers presented experimental data on the mean flow profiles and they observed that the shape of the unsteady component of the pulsating velocity profile depends on the frequency parameter. Essentially, there exist two frequency parameters of interest, ω' and ω_t', in pulsating flow studies. The first remains constant and can be thought of as the ratio of two times, the time of molecular diffusion over a radius R, divided by the period of pulsation, T_o. The second, ω_t', which represents the ratio of turbulent diffusion time to the pulsation period, changes value over the radius since ε depends on spatial location. Denote these as the viscous and turbulent times; except near the wall, the viscous time is much larger than the turbulent time because $\varepsilon >> \nu$. Hence, when the flow is turbulent at all times during the pulsation cycle, the turbulent mechanism is expected to be the dominant transfer mechanism for the pulsating component except very near the wall where ε is effectively damped out. Now, as the pulsation time, T_o, is very large, the turbulent diffusion time is small compared to T_o and the oscillating velocity profile is expected to follow a turbulent distribution at all times during a cycle; i.e., as suggested by Gerrard the oscillating profile follows a $(1-y)^{1/n}$ distribution from center-line to the wall. As the pulsation time, T_o, is small, the turbulent diffusion time is large compared to T_o and Gerrard and Karlsson show that there exists in the oscillating velocity profile a uniform speed region over the center part of the pipe.

Nonstationary turbulence in periodic turbulent pipe flow was also studied by Cheng (5). However, there is evidence indicating that Cheng's measurements were not made in a fully developed turbulent flow. The distance from the test section to the tripping ring was only about 16 pipe diameters. Furthermore, Cheng compared the velocity profile of stationary flow $Re_s = 5.97 \times 10^4$ with Laufer's (10) data at $Re_s = 4.05 \times 10^5$ instead of 4.05×10^4. This indicates that Cheng's flow is plug like and not fully developed.

Most of the preceeding studies provide a hydrodynamic view of the effect of pulsations on turbulent flow. Little is known about the behavior of the turbulence structure. Benson (2) measured the axial pulsating turbulent intensity at the pipe centerline in a water system at a mean flow Reynolds number of 10^4, with frequencies of 0.5 to 1.6 cps, and with pulsation amplitudes up to 0.45. He concluded that the overall effect of pulsing the flow on the centerline turbulence level is small. The axial pulsating turbulence intensity averaged over several imposed pulsation cycles differed from the steady turbulent flow value by a maximum of $\pm$ 5%. Within experimental error, Karlsson (8) also found that there is no effect of pulsations on the long time averaged axial turbulent intensity.

Information about the instantaneous pulsating turbulent characteristics is very limited. By observing the recorded instantaneous turbulent signal, Benson (2) and Gerrard (7) noted that the turbulence intensity generally decreased during the acceleration period and increased during the deceleration period.

The purposes of the experimental investigation reported upon here were:

1. To study the suitability of making measurements of turbulence properties in pulsating water flow using the constant temperature, hot-film anemometer.

2. To determine the effects of pulsations on fully developed turbulent pipe flow in order to shed some light on the frequency response in the intermediate frequency regime with pulsations of a significant but small amplitude compared to the mean flow so that mean flow reversals do not occur. These studies were made coincident with and complementary to a more detailed measurement of statistical properties of such flows in air (16).

3. To compare experimental results with the predictions of a model developed by Lu and Nunge (13,14). Experiments were run for the parameter ranges $16000<Re_s<81600$, $0\leq G_u/G_s\leq 8.4$, and $0\leq\omega'\leq 3130$. These dimensionless quantities for water flow correspond to a real frequency of 0 to 0.7 cps and centerline velocity amplitudes of 0 to 25% of the mean flow.

EXPERIMENTAL APPARATUS

The experimental system was designed so as to insure that the quantities of interest were measured in the fully developed region of the pipe flow. Two types of flow were generated, one in which the flow was steady, and the other in which the flow was varied in a periodic manner. The equipment consisted of a water loop system, a pulsation generator, a hot-film probe calibrating tank, and the electronic equipment for turbulence measurements.

Flow System

The major features of the water loop are shown schematically in Figure 1 and its detailed description is given in (13).

Since water purity is essential in this study, non-corrosive materials were used to construct the flow loop. Plastic pipes, valves, and fittings were selected for the construction of the test section and auxiliary lines. All wetted metal parts, such as the rotameter float, pump, and tank were made with 316 stainless steel and Epoxy coated steel.

Steady flow was maintained by gravity feed from a constant head tank located 28 ft. above the exit constant head tank. A constant head was achieved by placing a baffle with an overflow in the tank, and by keeping the flow rate in the return line 2, greater than in the feed line 1. The water loop was closed by a 5 hp centrifugal pump in the return line, and by connecting an overflow line 3, between the two constant head tanks. The flow rate was controlled by a diaphram valve and read out from a rotameter.

A one-foot long section of the inlet pipe was lined with #40 mesh stainless wire screen followed by a 1/16-inch high tripping ring to aid flow development. The flow development and test sections were constructed with four lengths of 2-inch I.D. and 2.5-inch O.D. Cast Acrylic Resin Tube supplied by Kaufman Glass Company. The ends of these tubes were carefully squared, and then joined together by four tightly fitting slip couplers and sealed with silicone. The test stations were located at 34, 55, 79 and 83 pipe diameters away from the end of the ring, respectively. The third station, which has a distance 79 pipe diameters from the end of the tripping ring was the main station where the velocity and turbulence measurements were taken.

A system for calibrating hot-film probes in water was located near the exit head tank. This system consisted of a 10-inch diameter by 28-inch high acrylic tank and a PVC controllable overflow unit. The water was fed into the calibrating tank from the upper constant head tank, and discharged to the exit constant head tank. The nozzle for the water jet was carefully designed to prevent separation

between the flow and the nozzle wall, and to ensure that the flow fills the throat. The probe was placed in the water jet at the nozzle exit for calibration at constant velocity.

The pulsations were generated by a MRI-79-92 SM Simplex Milroyal pump which has a plunger diameter of 2-1/2 inches. The pump stroke could be varied between 0 to 3 inches and its frequency between 16 to 92 cycles per minute. The suction and discharge check valves were removed in order to prevent any net pumping.

A number of precautions have been taken in preparing the water to prevent drift in the anemometer readings. Distilled water was used throughout the loop and a filter and ion exchange unit was used in the return line to maintain water purity and to remove solid particles down to 1-3 microns.

Part of the data (Reynolds stress) was measured in an air flow system with a 6-inch inside diameter pipe. For the detailed structure of the air system, the reader is referred to (16).

Measurement System

The major components of the measurement system for pulsating turbulence measurements are shown schematically in Figure 2.

Turbulence measurements were made with DISA equipment. A fiber film probe 55F09 was used in the velocity and axial turbulence intensity measurements and a DISA 55F07 45° slanting sensor type fiber probe was used in the Reynolds stress measurements. The probes were operated by a linearized DISA constant temperature anemometer system. The anemometer outputs were partially processed in a Kohn Hite filter, model 3323, and the various outputs either recorded on a Clevite 15 two-channel recorder or read directly from appropriate voltmeters.

The root mean square value was read out from a TSI Model 1060 RMS meter. This unit provides a maximum time constant value of 100 sec.

The wall static pressures of the steady and pulsating flows were measured by a Kistler Model 311 pressure transducer. This pressure transducer is basically a D.C. device but has a perfect frequency response up to 10 Hz.

MEASUREMENT TECHNIQUE

Data Reduction

Before proceeding to the discussion of the techniques used in reducing the experimental data, it is useful to distinguish between the terms "short-time" average and "long-time" average, each of which refers to time-averaging of mean and turbulent signals.

There are two time scales of concern in the pulsating flow experiments: the time scale of the turbulent fluctuations and the time scale of changes in the mean velocity. All of the experiments and the analysis have been done for the case in which the time scale of changes in the mean velocity is much larger than the time scale of the turbulent fluctuations. Hence, short-time averaging means averaging over the time scale characteristic of the turbulent fluctuations. For example, the short-time average of u is zero, but the short-time average of the total velocity is the mean velocity which, in the case of pulsating flow, is time dependent. The long-time average is an average over the period of pulsation; thus the long-time average mean velocity is independent of time.

Linearized probes were used to make the turbulence measurements. Thus the instantaneous voltage output from the anemometer is linearly related to the instantaneous velocity, V, through

$$E_e = KV \ , \qquad (1)$$

where K is a constant determined from the calibration and V is the velocity causing heat transfer from the probe sensor.

The following relation is obtained for long-time averaging:

$$\bar{\bar{E}}_e = K\bar{\bar{U}}_1 \ , \qquad (2)$$

where the double overbar indicates a long-time average. Equation 2 indicates that the base velocity upon which the pulsations and fluctuations are imposed can be obtained by finding $\bar{\bar{E}}_e$, which in practice is achieved by processing the anemometer signal

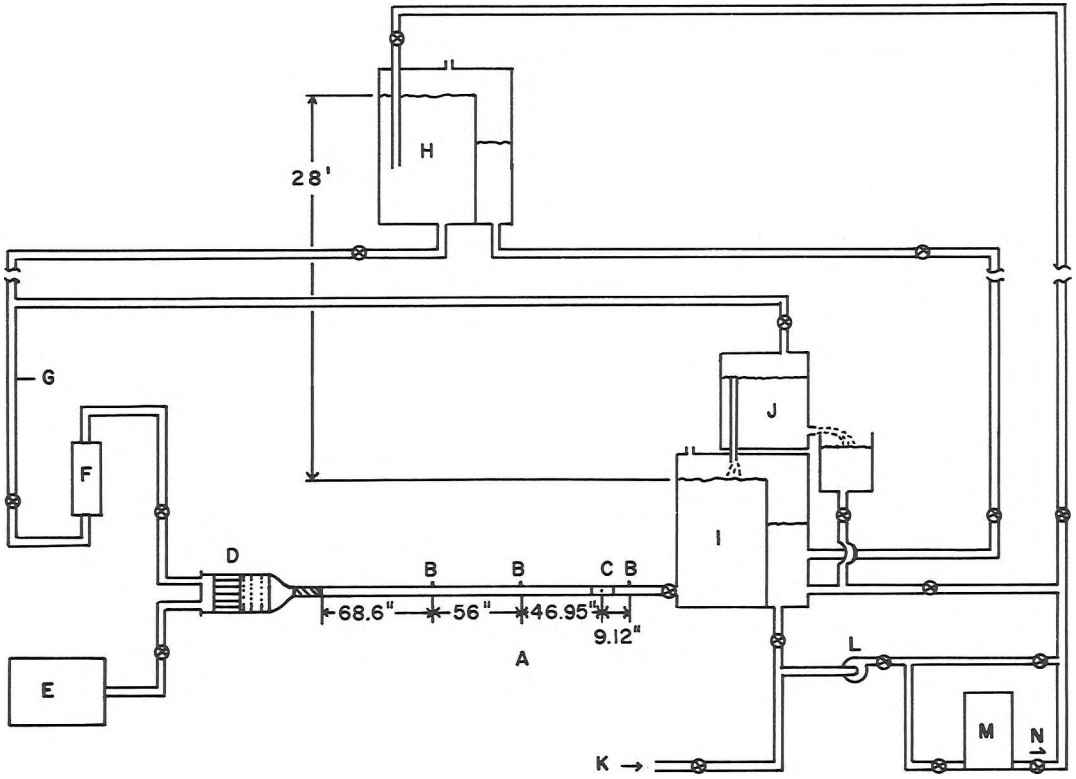

Key to Figure 1:

A	Test Section; 2" i.d. pipe	H	Constant Head Inlet Tank - 200 gal.
B	Pressure Taps	I	Constant Head Exit Tank - 200 gal.
C	Velocity Probe Station	J	Calibration Tank
D	Calming Chamber	K	Water Makeup Line
E	Reciprocating Pump	L	5 Hp. Centrifugal Pump
F	Rotameter	M	Filter and Ion-Exchanger
G	Thermometer	N	Check Value

Figure 1. Schematic diagram of the water flow system.

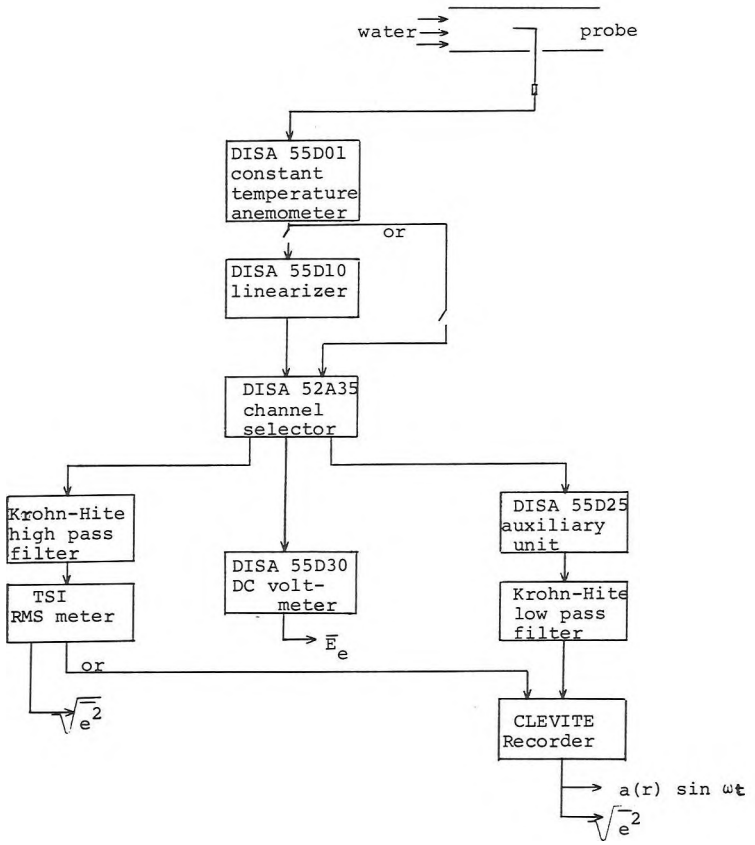

Figure 2. Flow diagram illustrating the electronic processing of the probe signal.

through a D.C. voltmeter with a high damping factor. The results of these measurements (see Figures 3 and 4 for examples) indicate that U_1 is coincident with the steady flow velocity distribution at the same mean Reynolds number such that the instantaneous velocity in the axial direction U can be written as

$$U = U_s(r) + U_t(\omega t, r) + u \qquad (3)$$

where $U_s(r) = \underline{\underline{U}}_1$ and U_t is the pulsating velocity component superimposed on the base flow.

In order to recover the pulsating component of the axial velocity, U_t, from the anemometer signal, it is necessary to suppress the portion of the signal due to U_s and u. Since U_s produces $\underline{\underline{E}}_e$, it is a simple matter to subtract this part. With pulsations at a known frequency ω, the main contributions of u were attenuated electronically by filtering. The signal was low-pass filtered to remove all input having a frequency above the known frequency of pulsations. In practice, the cutoff frequency for the low-pass filter was set at some value $n\omega$ where $n>1$.

Two errors are introduced in the resultant recordings of U_t by the filtering. These are the attenuation of the amplitude of the pulsations and a phase shift. The amount of attenuation and phase shift is a function of the cutoff frequency set on the filter. For large values of n, less attenuation occurs but more contributions from the turbulent fluctuations are evident in the recorded signal. To correct for the attenuation, the filter was calibrated using a sine wave generator. The attenuation factors for the cutoff frequencies used in the low-pass filtering at various pulsation frequencies were obtained. The attenuation factor is defined as the ratio of the peak-to-peak voltage of the sine wave after filtering to that before filtering. The attenuation factor which is independent of the input voltage, was used to correct the recorded values of the imposed pulsations.

The phase shift effect of the filter can be determined by using the Clevite recorder to mark on the recording paper whenever the piston of the reciprocating pump goes to a peak position.

The value of U_t was sinusoidal over most of the pipe radius except near the wall. It is probable that distortions are due to the increased intensity of the turbulent fluctuations below the cutoff frequency as the wall is approached.

In order to obtain reproducible data, the velocity at a particular radial location for a particular time in a cycle was arrived at by averaging the values for several cycles of pulsation. Determination of the number of cycles required led to adopting an averaging over 10 cycles near the center line, over 20 cycles close to the wall and over 15 cycles in the region between.

The phase shift caused by the filtering is critical in determining the phase relationship between the pressure and the pulsating velocity. Thus, to determine the phase difference between the center line velocity and the wall pressure, both signals were recorded simultaneously without filtering. The phase lag of the center line velocity could then be used as a reference value to determine the phase lag at other radial locations. These determinations are relatively inaccurate because of the small differences in the phase of the velocities at different radial locations.

In order to obtain the unsteady turbulent quantities, the imposed velocity variations have to be removed, since the amplitude of the pulsations is much larger than the amplitude of the turbulent fluctuations. The response equations for the axial turbulent intensity and the Reynolds stress measurements are

$$\overline{e^2} = K^2(\overline{u^2} + \overline{2ua \sin \omega t} + \overline{a^2 \sin^2 \omega t}) \qquad (4)$$

and

$$\frac{\overline{uv}}{U_s^2} + \frac{\overline{va \sin \omega t}}{U_s^2} = \frac{1}{4}\left(\frac{\overline{e_1^2}}{\underline{\underline{E}}_1^2} - \frac{\overline{e_2^2}}{\underline{\underline{E}}_2^2}\right) \qquad (5)$$

The interaction and sinusoidal terms in Equation 4 and the interaction term in Equation 5 can be removed by passing the signal through a high pass filter which attenuates the frequency ω. In practice, the cutoff frequency on the filter has to be

set at $n\omega$ where n has a value between 5 and 10 depending on the value of ω. Since this filtering is necessary in order to yield results for the turbulence structure itself, it was decided to compare the pulsating flow data obtained in this manner with steady flow results filtered in the same way. Thus the two could be compared on the same basis. This, of course, ignores the changes in the low frequency structure of the flow by the pulsations. The possibility existed for band pass filtering of the signal; i.e., processing the signal through both a high and low pass filter. However, unless a more efficient filter was used, this would not be effective. Since the results to be discussed do not show any startling differences between the steady and pulsating results for the axial turbulence intensity, the present techniques were felt to be adequate.

Since only the short-time average mean pressure gradient is of interest in this study, the pressure signal from the pressure transducer was low pass filtered to remove the turbulent pressure fluctuations above the known frequency of the pulsations. As discussed before, a correction factor for the attenuation was obtained by comparing the sine wave signal before and after passing through the filter. Within the experimental error, estimated at $\pm 5\%$, the results of the pulsating pressure measurements indicate that the steady component of the pressure gradient in the unsteady flow is coincident with the steady flow pressure gradient at the same mean Reynolds number. By recording the pulsating pressure component at three locations, it was possible to show that its amplitude has a linear relation with the axial distance in the fully developed region. The amplitude of the unsteady component of the pressure gradient during one cycle can be calculated from the slope of the straight lines. Therefore, the instantaneous pressure gradient can be written as

$$\frac{\partial P_1}{\partial z} = G_s + G_u \sin \omega' \tau \qquad (6)$$

A single slanting sensor type probe was used to measure the Reynolds stress. Unfortunately, the measurements were not satisfactory (13) and Reynolds stress data in a pulsating air flow system are reported instead (16).

Experimental Techniques

A problem of probe drift was observed in this study even though distilled water and a mechanical filter were used in the flow system. It is believed that the drift was caused by suspended particles smaller than about 2 microns, because the filter can remove particles down to this size. The effect of drift on the measurements was observed in the following manner: If measurements started at the pipe center line, a different voltage output was obtained from the anemometer when the probe was relocated at the pipe center after a few measurements at other radial locations. However, it was found that the resulting drift is less than 5% if the operating time of the probe was less than about 25 min. The original calibration curve of the probe could be reestablished within $\pm 3\%$ if the probe was cleaned with a fine brush and agitated in acetone. The procedure used was to check the output voltages with the film located at the pipe center every 20 minutes. If the readings were within 3% of those obtained when the film was clean the experiment was continued. If the error was more than 3% but less than 5%, the film was taken out and cleaned before proceeding. If more than 5%, the film was taken out for cleaning and the data of the last 20 minutes were discarded.

Before proceeding to discuss the results, it is worthwhile to make clear the meaning of the term "side-by-side run". It will be seen that the effect of pulsations on turbulent structure is small in the parameter range studied here. Unfortunately scatter in the data is of the same order of magnitude as the effects introduced by the pulsations and the results are thus difficult to analyze. The data acquisition was improved, and the data scatter was reduced by taking measurements in the following manner: one unsteady flow measurement was taken at a fixed position and then one steady flow measurement was taken at the same position and at a Reynolds number equal to

the time averaged mean Reynolds number of the unsteady flow; finally an attempt was made to reproduce the unsteady flow quantity at the same parameters as the first measurement. About 5 minutes elapsed between each measurement to allow the turbulence to become fully established. The data were accepted only when the first data point was reproduced by the third measurement. This procedure is termed a "side-by-side run",

MODELING PULSATING FLOW

If one adopts an eddy diffusivity approach to modeling turbulence then one is faced with the critical question of the form of the eddy diffusivity in pulsating flow. It seems physically reasonable that in the limit of small frequency, the turbulence would follow a quasi-steady behavior and the instantaneous eddy diffusivity distribution could be determined from the time-dependent Reynolds number of the flow and the eddy diffusivity for steady flow as a function of the Reynolds number. Furthermore, if the amplitude of the pulsations is restricted to small values, then variations of the Reynolds number with time can be ignored since the steady state eddy diffusivity is known to be relatively insensitive to the Reynolds number. These assumptions were made in the present work and the Cess' expression for the eddy diffusivity (3,13) was used for computational convenience. The extent to which the model predictions agree with experimental measurements of the pulsating velocity component is explored subsequently.

The sinusoidal pressure gradient given by Equation 6 is the forcing function of the flow. Under the present assumptions, the short-time averaged equation of motion can be written as:

$$\frac{\partial u_1}{\partial \tau} = \frac{1}{y}\frac{\partial}{\partial y}\left(y\left(1+\frac{\varepsilon}{\nu}\right)\frac{\partial u_1}{\partial y}\right) - \frac{\partial P_1}{\partial z} \tag{7a}$$

$$u_1(0,y) = u_s \tag{7b}$$

$$u_1(\tau,1) = 0 \tag{7c}$$

$$\frac{\partial u_1}{\partial y}(\tau, o) = 0 \tag{7d}$$

The linearity of Equation 7 allows one to divide the pulsating turbulent flow velocity into two parts: a steady part upon which the pulsations and fluctuations are imposed and an unsteady part which is affected by the pulsations. Thus,

$$u_1 = u_s(y) + u_t(\tau,y) \tag{8}$$

Upon substituting Equations 6 and 8 into Equation 7, the result can be solved by using the Duhamel theorem and separation of variables. The expressions for the two parts of the short-time average velocity are given below; details of the solution are given in Reference (13).

$$u_1 = \frac{1}{2}G_s\int_1^y \frac{y}{1+\varepsilon/\nu}\,dy + \sum_{n=1}^{\infty} \frac{\alpha_n^2 Y_n\left[\int_o^1 \left(\int_1^y \frac{y}{1+\varepsilon/\nu}\,dy\right)Y_n y\,dy\right]}{\int_o^1 y Y_n^2\,dy} \times \frac{G_u(\alpha_n^2\sin\omega'\tau - \omega'\cos\omega'\tau]}{(\alpha_n^2)^2+(\omega')^2}, \tag{9}$$

where α_n^2 is the nth eigenvalue and Y_n is the nth eigenfunction, which satisfy

$$\frac{d}{dy}y(1+\varepsilon/\nu)\frac{dY_n}{dy} + \alpha_n^2 y Y_n = 0 \tag{10a}$$

$$Y_n(1) = 0 \tag{10b}$$

$$\frac{dY_n}{dy}(0) = 0 \tag{10c}$$

Equation 9 has been successfully used to predict the dispersion phenomena in pulsating turbulent pipe flow (14).

A useful relationship between the bulk velocity and the pressure gradient can be obtained from a simple derivation. In the quasi-steady regime, by space-averaging the equation of motion, one obtains

for the short-time averaged velocity

$$\frac{1}{\rho}\frac{\partial P}{\partial x} + \frac{\partial \bar{U}(t)}{\partial t} + \frac{f\bar{U}^2(t)}{2D} = 0 \qquad (11)$$

The friction factor can be evaluated from the steady flow equation using the instantaneous bulk velocity. If the Blasius equation is used, one has

$$f = 0.3164\left[\frac{\nu}{D\bar{U}(t)}\right]^{0.25} \qquad (12)$$

Let us assume that the bulk velocity has a sinusoidal form

$$\bar{U}(t) = u_o + B\cos\omega t \qquad (13)$$

where u_o is the steady component of the bulk velocity and B is the amplitude of the bulk velocity variation. The steady component satisfies

$$0 = -\frac{1}{\rho}\left(\frac{dP}{dX}\right)_s + \frac{f_s u_o^2}{2D} \qquad (14)$$

If Equations 12 and 13 are substituted into Equation 11 and Equation 14 is subtracted from the result, one obtains

$$-\left(\frac{1}{\rho}\frac{\partial P}{\partial X} - \frac{1}{\rho}\left.\frac{\partial P}{\partial X}\right|_s\right) = -\frac{1}{\rho}\left.\frac{\partial P}{\partial X}\right|_t \qquad (15)$$

$$= A u_o\omega \sin\omega t + C u_o^{1.75}(1.75A\cos\omega t + 0.656A^2\cos^2\omega t + \ldots.)$$

where

$$C = 0.1582D^{-1.25}\nu^{0.25}$$

If the amplitude of the pulsating velocity is small enough relative to the steady component of the bulk velocity, such that A^2 and higher order terms can be neglected relative to A, Equation 15 becomes

$$B(\omega\sin\omega t + 1.75\,C\,u_o^{0.75}\cos\omega t) = -\frac{1}{\rho}\left.\frac{\partial P}{\partial X}\right|_t \qquad (16)$$

It can be seen from Equation 16 that a linear relation exists between the amplitude of the unsteady component of the bulk velocity and the amplitude of the unsteady component of the pressure gradient.

RESULTS AND DISCUSSION

Mean Flow Structure

Figures 3 and 4 show the dimensionless long-time average mean velocity and the steady flow velocity measured at the same mean Reynolds number plotted versus dimensionless radial distance. Within experimental error, the two experimental velocity profiles are the same, thus indicating that over the parameters studied, the mean Reynolds number determines the base flow velocity upon which the pulsations are superimposed.

Figures 3 and 4 also show the velocity distribution for steady flow predicted using the eddy viscosity of Cess. For Re_s=45,000 the predicted velocity profile is somewhat high (3%) over a part of the radius; for Re_s=81,600, the agreement is better across the entire radius. Absolute agreement is not to be expected, but the deviations at lower Reynolds numbers evident in Figure 3 may have some effect on the extent to which the eddy-viscosity model is able to predict the pulsating velocity. We will return to this point later.

The quasi-steady model developed here suggests that u_t/G_u is independent of G_u, as shown in Equation 9. The experimental results of the dimensionless ratio of unsteady velocity and pressure gradient are shown in Figure 5 at Re_s=45,000, ω'=1,336 and G_u/G_s=0.253, 0.760, and 1.265. Various times over a pulsation cycle are plotted as a parameter. Within experimental error, the experimental data in Figure 5 indicate that u_t/G_u is independent of G_u. This finding agrees with the result of Karlsson (8). It is also to be noted on Figure 5 that the distribution of velocity shows only qualitative agreement with the predictions of the model; this will be discussed later.

It has been shown in Equation 16 that a linear relation between the amplitude of the unsteady component of the bulk velocity and the amplitude of the unsteady component of the pressure gradient can

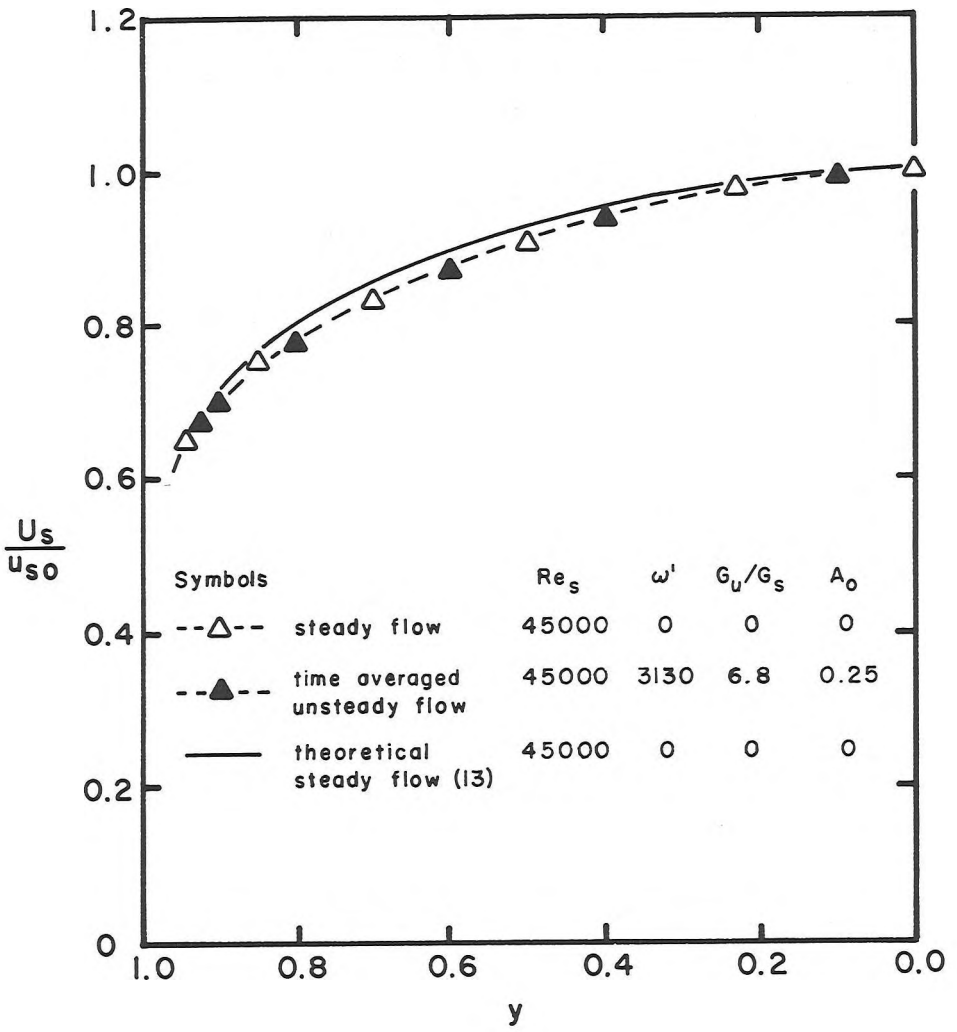

Figure 3. The dimensionless velocity versus the dimensionless radial distance for several sets of parameters.

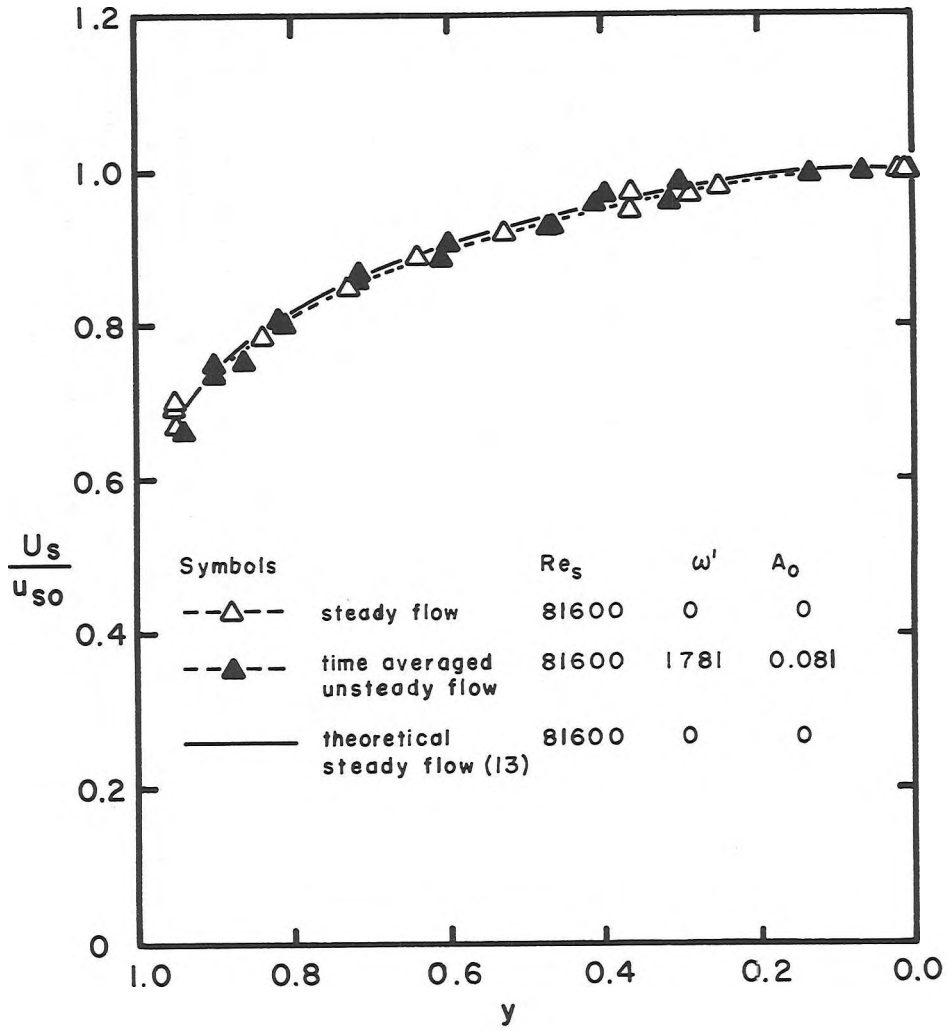

Figure 4. The dimensionless velocity versus the dimensionless radial distance for several sets of parameters.

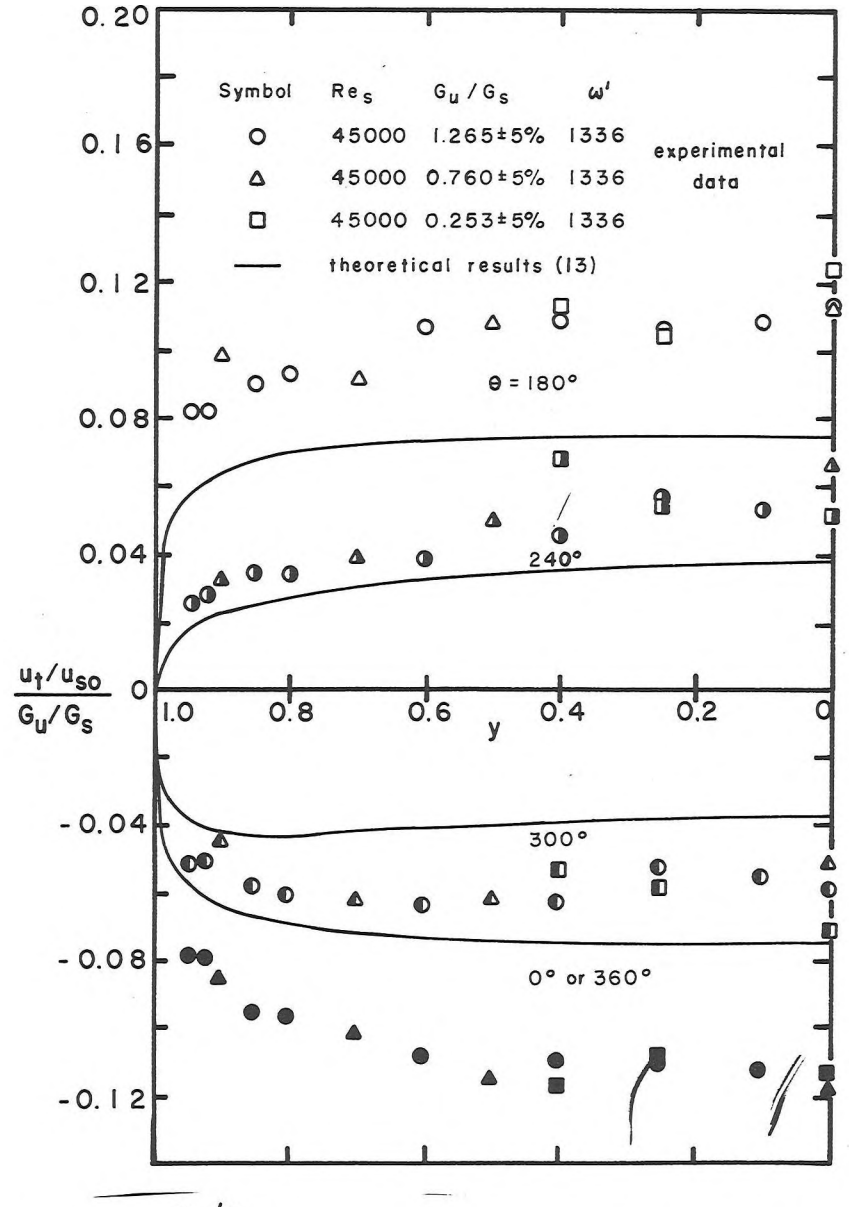

Figure 5. $\left(\frac{u_t/u_{so}}{G_u/G_s}\right)$ versus y for Re_s=45,000, ω'=1,336 and G_u/G_s=0.243, 0.760 and 1.265.

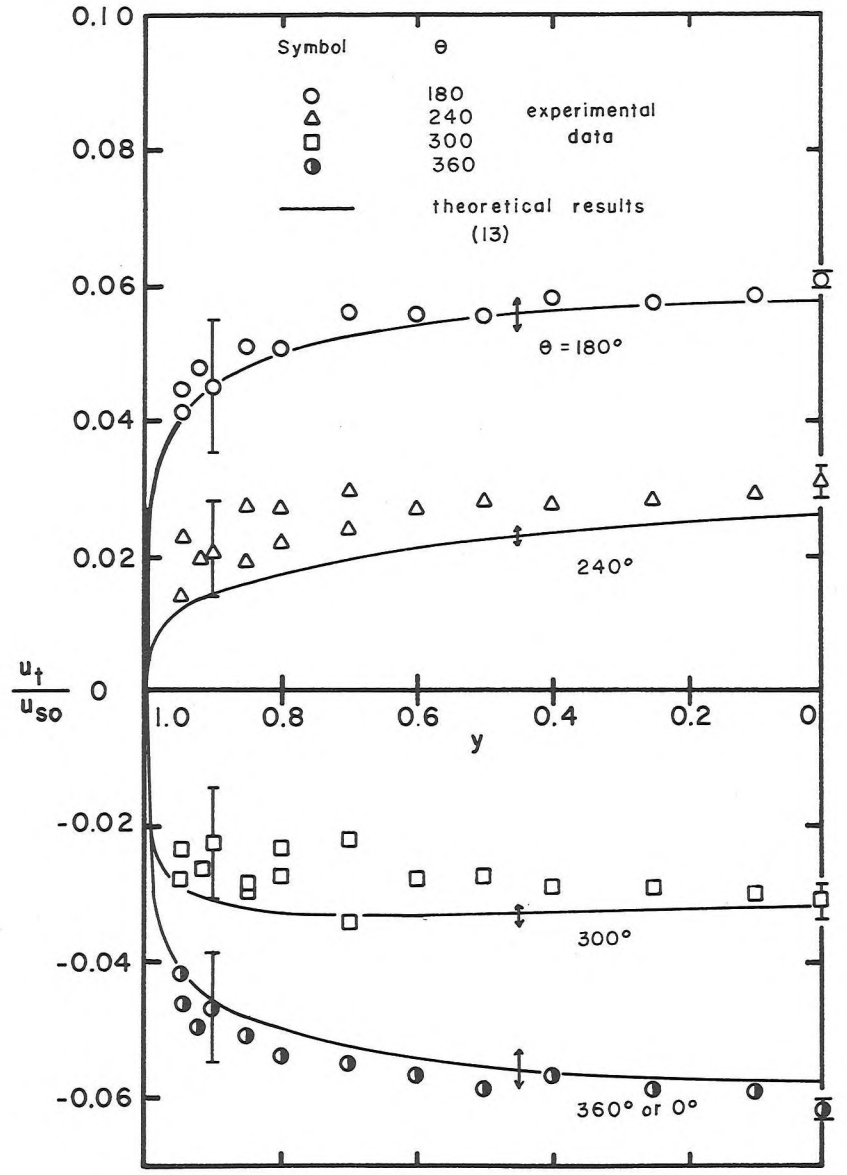

Figure 6. u_t/u_{so} versus y for Re_s=81,600, G_u/G_s=0.43 and ω'=1,291 with θ as a parameter.

exist only when the pulsating velocity is small enough relative to the steady component of the velocity. Thus, Equation 15 indicates that at some point the amplitude of the unsteady pressure gradient becomes an important parameter. For the range of amplitudes covered in this study, the second order term dropped in formulating Equation 16 does not exceed 5% of the first order terms retained. No experiments were made in the large amplitude range because of limitations of the available equipment.

Figures 6 to 9 show comparisons between the pulsating component of the velocity obtained by experiment and from the model at different times in a pulsation cycle. The angle designations θ correspond to a cycle of the sinusoidal pressure gradient. It can be seen that in Figures 6 and 7, the deviation between the theoretical and experimental results is about 5% at the peak centerline velocity, but in Figures 8 and 9 the deviation is more than 25% at the peak centerline velocity. This suggests that different mechanisms, not considered in the model, are significant. Some possible reasons for the discrepencies are discussed in the following paragraphs.

The deviation between the theoretical and experimental results shown in Figures 6 and 7 may be due to the following reasons: 1) One assumption made in the theoretical analysis was that when the amplitude of the pulsation velocity was relatively smaller than the time-averaged mean velocity, the eddy diffusivity could be evaluated at the time-averaged mean Reynolds number instead of the instantaneous value. Unfortunately, the error involved in this assumption is impossible to determine analytically, unless the exact solution of the momentum equation with time-varying eddy viscosity is available. This error is not expected to be large, since the amplitude of the velocity variation is only 6 to 8% of the time-averaged mean velocity and it is well known that at high Reynolds numbers in steady flow, the mean velocity distribution is relatively insensitive to the Reynolds number. 2) The eddy diffusivity used in this analysis may introduce some deviation between the theoretical and experimental results. However, the 3% deviation existing in Figure 3 for the steady flow results shows a strong dependence on the position over the pipe cross section, but the deviations shown in Figures 6 and 7 are about the same over the entire pipe cross section. This suggests that the differences between Figures 6 and 7 are not entirely introduced by the eddy diffusivity function. 3) The measurement of G_u is accurate to within 5% which is indicated by an arrow on Figures 6 and 7 to show the effect of this uncertainty on the unsteady component of the velocity profile. 4) As an internal check of the consistency of the results, the area average pulsating velocity at its maximum value was checked against the maximum speed of the piston forcing the flow. From continuity these should be the same. It was found that about 7% systematic error is involved in the velocity measurements. It is believed that the differences between model and experiment evident in Figures 6 and 7 are entirely due to these factors. It is thus tentatively concluded that the quasi-steady model applies to pulsating turbulent flow under the conditions shown in these figures.

Figures 8 and 9 show that there is more than 25% deviation between the theoretical and experimental results for the conditions described in these figures. The factors discussed in the previous paragraph involved only small differences and therefore, it appears that the quasi-steady model is no longer applicable.

Table 1 summarizes the parameters which were used by various investigators to study the quasi-steady model in pulsating turbulent flow. It can be seen from the table that the formula suggested by Brown, $0.01\ Re_s > \omega'$, underestimates the range over which the quasi-steady model applies. The following equation gives a better estimate of the range in which quasi-steady model applies:

$$0.025\ Re_s > \omega' \qquad (17)$$

It is believed that the differences between the experimental data and theoretical model illustrated in Figures 5, 8, and 9 are due to frequency

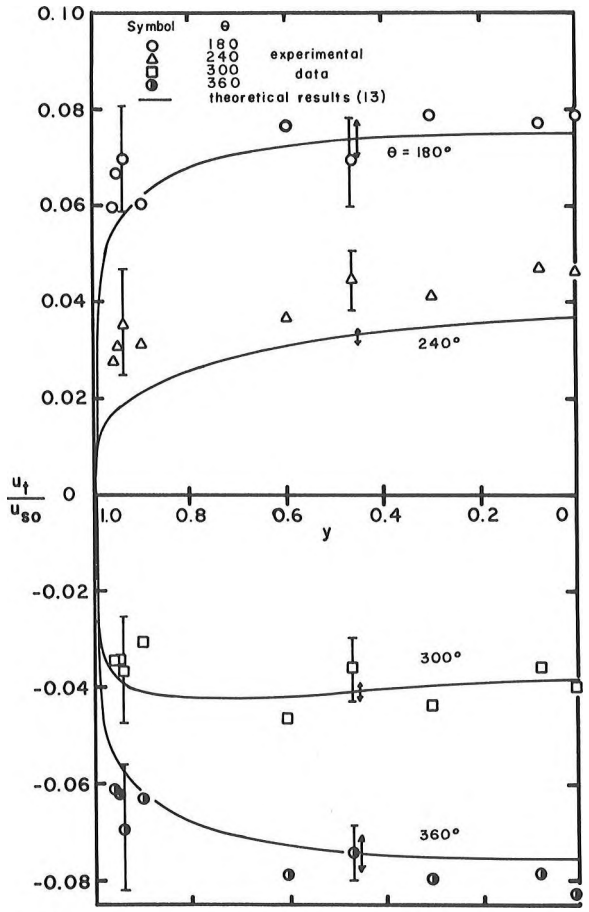

Figure 7. u_t/u_{so} versus y for Re_s=81,600, G_u/G_s=0.79 and ω'=1,781 with θ as a parameter.

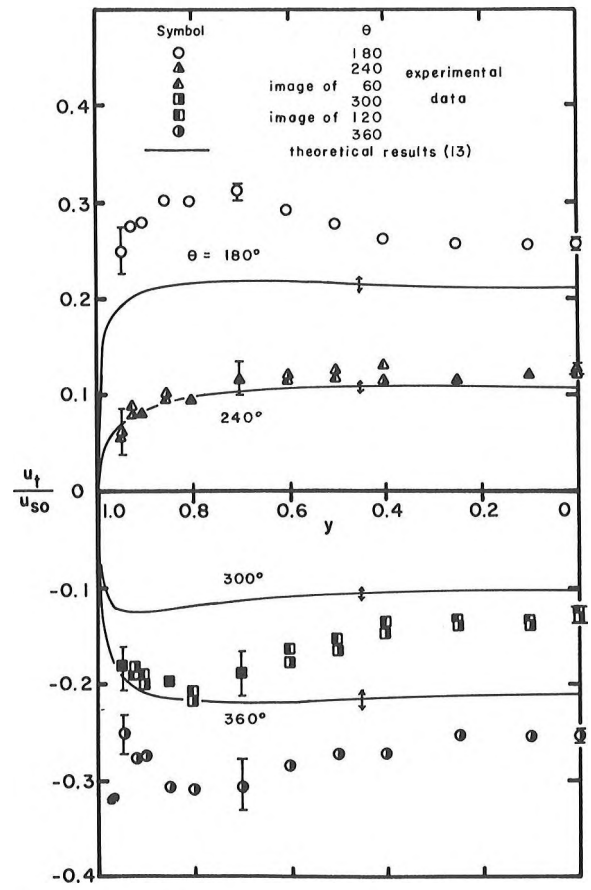

Figure 9. u_t/u_{so} versus y for Re_s=45,000, G_u/G_s=6.80 and ω'=3,130 with θ as a parameter.

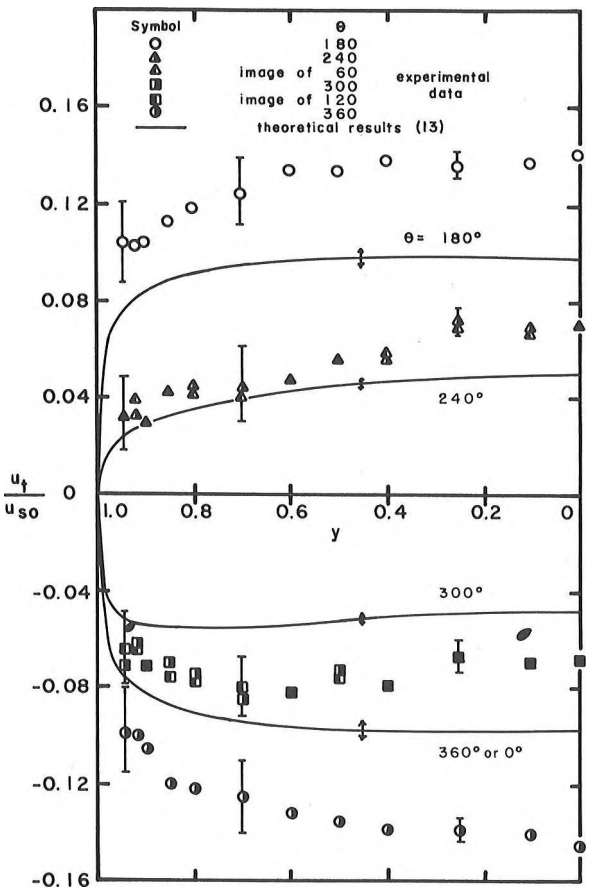

Figure 8. u_t/u_{so} versus y for Re_s=45,000, G_u/G_s=1.265 and ω'=1,336 with θ as a parameter.

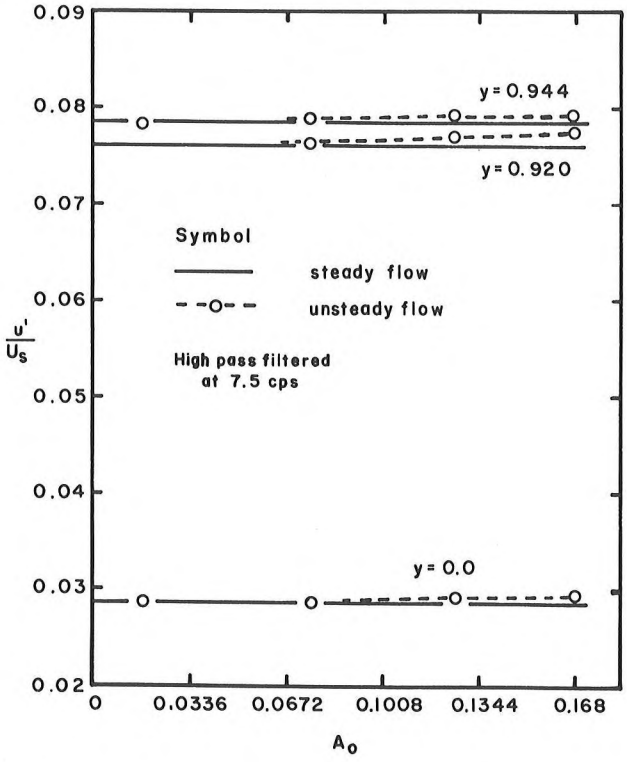

Figure 10. The effect of pulsating amplitude on the axial turbulent intensities for Re_s=81,600 and ω'=4,140.

Table 1. A comparison of known experiments with pulsating turbulent flow.

	Brown et al (4)	Baird et al (1)	Schultz-Grunow (17)	Schultz-Grunow (17)	Schultz-Grunow (17)	Present Measurements				Mohajery (16)		
						Water System	Water System	Water System	Water System			
Re_s		17,000	57,000	47,000	77,000	81,600	81,600	45,000	45,000	20,000	90,000	90,000
0.01 Re_s	range in which quasi-steady model applies	1,700	570	470	770	816	816	450	450	200	900	900
.025 Re_s	break point	4,250	1,425	1,175	1,925	2,040	2,040	1,125	1,125	500	2,250	2,250
maximum ω' studied		2,848	1,078	1,078	1,724	1,291	1,781	1,336	3,130	2,255	1,216	2,255
quasi-steady model applies		X	X	X	X	X	X				X	
quasi-steady model does not apply								X	X	X		X

range of the experiments which is outside the quasi-steady range suggested by Equation 17. If this is the reason for the deviations between the model and experiment, then it can be concluded from Figure 5 that for amplitudes within the range studied here, the amplitude of the pulsation is not a significant parameter inside or outside of the quasi-steady frequency range.

It is also believed that the model should be able to predict the flow behavior in the "frozen" viscosity, or high frequency, region as suggested by Brown. In essence, we have assumed that the pulsating velocity component is governed by the turbulent diffusion mechanism. Since the instantaneous Reynolds number does not change over wide ranges, it is assumed that the eddy viscosity can be evaluated from the long-time averaged Reynolds number.

It can be seen from Figure 9 that the velocity profiles possess a plateau over the central region of the pipe. This phenomena may be explained qualitatively by the value of the frequency parameter, $\frac{R^2\omega}{\varepsilon}$, where R is the tube radius and ε/ω is the length scale of vorticity. This parameter measures the ratio of the tube radius to the distance through which vorticity produced at the wall will diffuse in one period of the pulsation. For simplicity, the cross-sectional mean-eddy diffusivity is replaced by the pipe center line eddy diffusivity ε_o. The calculated values of $\frac{R^2\omega}{\varepsilon_o}$ for the conditions studied in Figures 6 to 9 range from 9 to 40. The largest value is at the conditions studied in Figure 9; that is, at these conditions the tube radius is considerably larger than the distance through which vorticity produced at the wall will diffuse in one period of pulsation. Figure 9 shows that in the center part of the pipe, there exists a uniform speed region where vorticity never has time to diffuse before being annulled by oppositely signed vorticity.

Axial Turbulence Intensity

It was found that the pulsations have a small effect, less than $\pm 5\%$, on the long-time averaged axial turbulence intensity over the parameters studied in this work. This effect depends upon the following parameters: the time-averaged mean Reynolds number, pulsating frequency and amplitude, and radial distance.

Since the effect of pulsations on the turbulence intensity was small, only side-by-side runs can give conclusive results. The effect of amplitude on the axial turbulence intensity is shown in Figures 10 and 11 for different radial locations. A clear trend can be seen from these figures. The pulsation amplitude can intensify the effect of pulsations on axial turbulence intensity; i.e., at a particular set of conditions, if the local axial turbulent intensity is decreased by the imposed pulsations, it will be further decreased with increasing pulsating amplitude. If the local axial turbulence intensity is increased by the pulsations, it will increase with increasing pulsating amplitude.

Since only a small range of pulsating frequency, 0 to 1.0 cps, has been studied in this work, no significant effect of frequency on the axial turbulent intensity is observed.

Although the time variation of the turbulent intensity during the pulsing cycle was not measured, it was observed from the linearized anemometer signal that the intensity of the turbulent fluctuations is generally larger during deceleration than acceleration.

Reynolds Stress

The Reynolds stress measurements in this work were not successful as compared with Laufer's data for the steady flow case. The reason for the difficulties in the Reynolds stress measurements is not clear. The Reynolds stress measurements were obtained by a single wire inclined at 45° to the flow direction; thus two measurements were required to calculate the Reynolds stress at one radial position. This may introduce some error in the measurement (9, 15).

In order to complete the discussion, the Reynolds stress was measured using a x-wire probe in an air system. Excellent agreement with Laufer's data for steady flow was obtained. Figure 12 shows the effect of pulsations on the long-time-averaged Reynolds stress. The Reynolds stress of the pulsating flow turbulence was compared with the steady flow turbulence at the same long-time average parameters and both signals were high pass filtered at 2.5 cps which was sufficient to attenuate completely the main flow pulsations. It can be seen from this

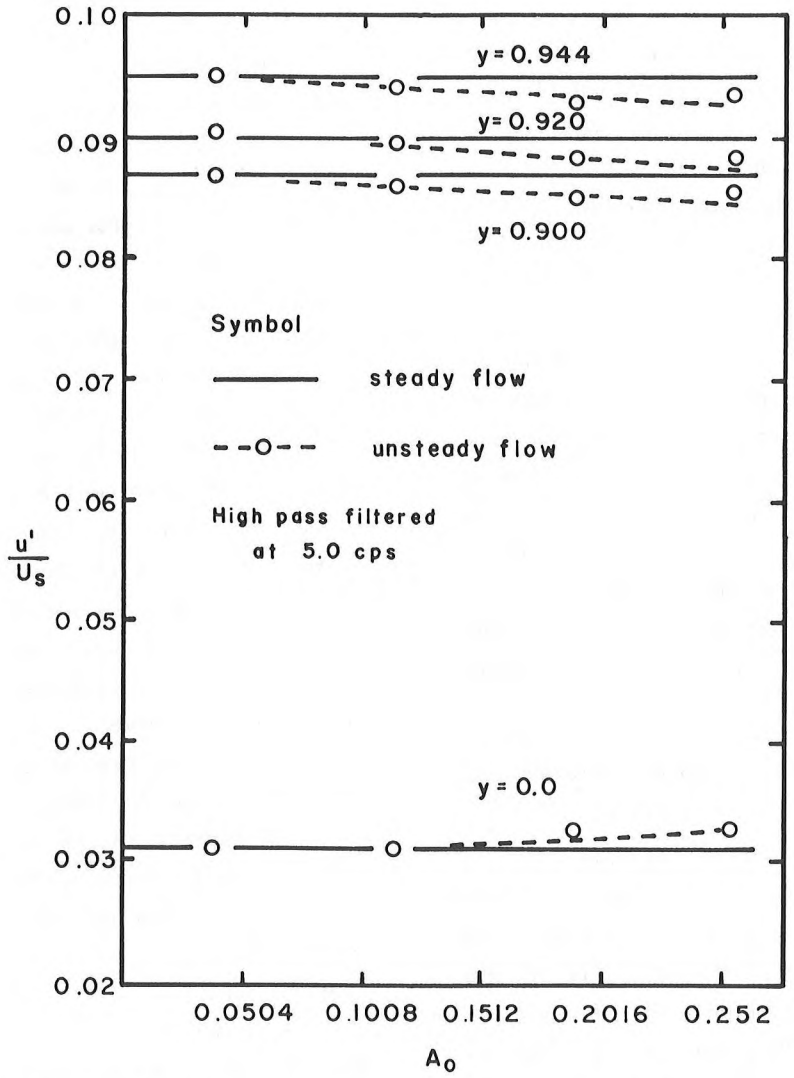

Figure 11. The effect of pulsating amplitude on the axial turbulent intensities for Re_s=45,000 and ω'=3.130.

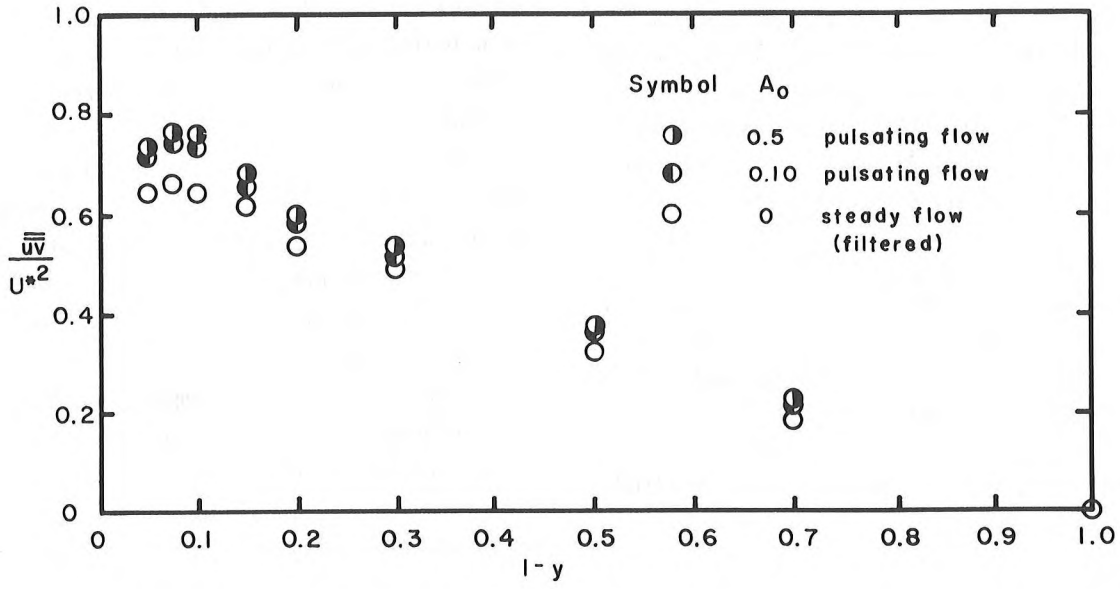

Figure 12. Distribution of the turbulent shear stress for steady flow (filtered) and pulsating flow at Re_s=80,500, and ω'=2,305. Measurements taken in air (16).

figure that an increase of up to 9% near the wall region is observed for the pulsating flow over the steady flow values.

One can show easily that the long-time averaged momentum equation for pulsating turbulent flow satisfies

$$\overline{\overline{uv}} = \nu \frac{d\bar{U}}{dr} - \frac{R}{2\rho} \frac{d\bar{P}}{dX} \qquad (18)$$

It was concluded previously that the long-time-average mean velocity $\bar{U}$ for the pulsating flow is equal to $\overline{U}_s$ (the base steady flow mean velocity), so that:

$$\frac{d\bar{U}}{dr} = \frac{d\overline{U}_s}{dr}$$

The long-time-averaged axial pressure gradient $\frac{d\bar{P}}{dX}$ is equal to the axial pressure gradient of the base steady flow. From Equation 18 one would conclude that the long-time averaged Reynolds stress $\overline{\overline{uv}}$ should be equal to the Reynolds stress in the base steady flow. Figure 12, however, shows that a small but definite increase is observed in the value of the long-time averaged Reynolds stress. This apparent inconsistency between the experimental results (especially at points near the solid boundary) and Equation 18 is not yet fully explained. The pressure measurements in this work are the least accurate of the measurements performed and are accurate to within $\pm 5\%$ by static calibration. It is then possible that the measured axial pressure gradient may be in error by as much as 10%. Equation 18 can be solved to obtain values of the pressure gradient using the measured values of the Reynolds stresses and long-time average mean velocity gradients and will result in higher long-time averaged axial pressure gradients (i.e., larger friction factors) for the pulsating flow than the steady turbulent flow at the same long-time-averaged Reynolds number.

CONCLUSIONS

The major conclusions drawn from this investigation are summarized below:

1. The quasi-steady model can be used to predict the hydrodynamic quantities of a pulsating turbulent flow system within the parameters range of of $0.025\ Re_s > \omega'$.

2. When the pulsating velocity amplitude is small compared to the mean velocity, the Reynolds number and the dimensionless pulsating frequency are the two critical parameters, whereas when the pulsating amplitude is not small compared to the mean velocity, the pulsating amplitude becomes an additional parameter.

3. At small values of $(\frac{R^2\omega}{\varepsilon_o})$, the profile of the unsteady component of velocity follows the turbulent flow type distribution. At large values of $(\frac{R^2\omega}{\varepsilon_o})$, the maximum velocity across the pipe moves from the center line to the region near the wall during part of the pulse cycle and a uniform speed region exists in the central part of the pipe.

4. The long-time averaged pulsating flow velocity is the same as the steady flow velocity at the same mean Reynolds number.

5. Over the parameters investigated in this study, pulsations have a small effect on the long-time averaged statistical turbulent quantities in the core of the flow. The pulsating amplitude can intensify the effect of pulsations on the axial turbulence intensity, but the pulsation frequency appears to have a negligible effect.

6. In agreement with previous work, the anemometer signal indicates that the magnitude of the turbulent velocity fluctuations are greater during deceleration than acceleration.

ACKNOWLEDGMENT

This research was supported by Atomic Energy Commission Contract No. AT(30-1)-4102 and National Science Foundation Grant GK-34539.

NOMENCLATURE

A dimensionless pulsating amplitude of the bulk velocity (B/u_o)

A_o the ratio of the pulsating amplitude of the center line velocity to the time-averaged center line velocity

a pulsating amplitude of the local velocity

B pulsating amplitude of the bulk velocity

D pipe diameter or diameter of the wire

E the bridge voltage, E_1 and E_2 are referred to the probe position

E_e the linearized anemometer output

$\overline{e^2}$ long-time mean-square voltage of u, $\overline{e_1^2}$ and $\overline{e_2^2}$ are referred to the probe position

f friction factor

f_s steady flow friction factor

G_s dimensionless steady component of pressure gradient

G_u dimensionless amplitude of unsteady component of pressure gradient

K a constant, defined in Equation 1

P_1 dimensionless pressure, $P/\rho u_o^2$

P time-smoothed pressure

R pipe radius

Re_s steady-flow Reynolds number or time mean Reynolds number for unsteady flow, $\frac{Du_o}{\nu}$

r radial coordinate from pipe center line

T_o period of pulsation

t time

U the mean local velocity

$\overline{U}(t)$ instantaneous bulk velocity

U_s long-time-averaged local velocity

U_t pulsating part of the local velocity ($a \sin \omega t$)

U_1 U_s+U_t

U^* friction velocity

u velocity fluctuation in the axial direction

u_1 dimensionless velocity, U/u_o

u' $\sqrt{\overline{u^2}}$

u_o steady-flow mean velocity or time-mean bulk velocity

u_s dimensionless steady flow velocity, U_s/u_o

u_{so} dimensionless steady flow velocity at pipe center line

u_t unsteady part of the dimensionless velocity, U_t/u_o

V the velocity causing heat transfer from the probe sensor

v velocity fluctuation in the radial direction

w velocity fluctuation in the angular direction

X axial coordinate

Y_n eigenfunction

y dimensionless radial distance from pipe center line, r/R

z dimensionless axial coordinate, $X\nu/u_oR^2$

α_n^2 eigenvalue

ε the steady flow eddy diffusivity

ε_o pipe center line eddy diffusivity

θ degree

ν kinematic viscosity

ρ density

τ dimensionless time, $t\nu/R^2$

ω frequency

ω' dimensionless frequency, $\frac{\omega R^2}{\nu_2}$

ω_t' dimensionless frequency, $\frac{\omega R^2}{\varepsilon}$

$\overline{}$ short-time-averaged quantity

$\overline{\overline{}}$ long-time-averaged quantity

REFERENCES

1. Baird, M. H. I., G. F. Round, and J. N. Cardenas, Can. J. Chem. Eng., 49, 220 (1971).

2. Benson, J. W., "Longitudinal Intensity of Turbulence for Pulsatile Flow in a Tube", M.S. Thesis, Dept. of Chem. Eng., Univ. of Washington (1968).

3. Blanco, J. A., "An Analytical Study of Single Stream and Multistream Turbulent Forced Convection Systems", Ph.D. Dissert., Dept. of Chem. Eng.,Syracuse Univ. (1967).

4. Brown, F. T., D. L. Margolis, and R. P. Shah, J. Basic Eng., 91D, 678 (1969).

5. Cheng, I.-M., "Nonstationary Turbulence in Periodic Turbulent Boundary Layers", Ph.D. Dissert., Dept. of Civil Eng., Univeristy of Utah (1971).

6. Denison, E. B., W. H. Stevenson, and R. W. Fox, A.I.Ch.E. J., 17, 781 (1971).

7. Gerrard, J. H., J. Fluid Mech., 46, 43 (1971).

8. Karlsson, S. K. F., J. Fluid Mech., 5, 622 (1959).

9. Knox, J. S., "Pipe Flow Turbulence", M.S. Thesis, Ohio State University (1966).

10. Laufer, J., NACA Rpt. 1174, 1954; Supercedes NACA TN 2954, 1953.

11. Lienhard, J. H., and C. L. Tien, ZAMP, 15, 375 (1964).

12. Linford, R. G., and N. W. Ryan, J. Appl. Physiol., 20, 1078 (1965).

13. Lu, S.-Z., "Pulsating Turbulent Water Flow in a Tube", Ph.D. Dissert., Dept. of Chem. Eng., Clarkson College of Technology (1972).

14. Lu, S.-Z., and R. J. Nunge, A.I.Ch.E. J., 17, 1001 (1971).

15. McKee, G. L., "Turbulence in Pipe Flow", M.S. Thesis, Ohio State University (1966).

16. Mohajery, M., "An Experimental Study of the Structure of Pulsating Turbulent Flow of Air in a Circular Pipe", Ph.D. Dissert., Clarkson College of Technology (1972).

17. Schultz-Grunow, F., Forschg. Ing.-Wesen, 11, 170 (1940).

18. Streeter, V. L. and E. B. Wylie, J. Eng. Power, 89A, 615 (1967).

19. Uchida, S., ZAMP, 7, 403 (1956).